Wiley Analytical Science

Specific Heat Capacity Determination by DSC

April 19, 10:00am - 11:00am EDT

Specific heat capacity (cp) is an important, temperature-dependent material property and is often specified in material data sheets. It is a key property for improving technical processes such as injection molding, spray drying, or crystallization, as well as for the safety analysis of chemical processes and the design of chemical reactors.

Watch this session during the WAS Virtual Conference:

Dr. Jürgen Schawe

Register Now

This talk is sponsored by METTLER TOLEDO

ADVANCED FUNCTIONAL MATERIALS
www.afm-journal.de

Exploration on Solvatochromic Sensing Probe of Phenol Blue for L-Lactic Acid Detection: Effective Strategy to Obtain Reliable Capacitive Sensor

Jungyoon Seo, Taehoon Hwang, Eun Ko, Seungtaek Oh, Dashdendev Tsogbayar, Md Rajibur Rahaman Khan, Jeong Ho Cho, Yeong Don Park, and Hwa Sung Lee**

This study systematically investigates a capacitive sensor applied with phenol blue (PhB)-based sensing medium for detection of L-lactic acid (LA), as a health monitoring indicator. PhB is a substance with solvatochromic effect, inducing the change in capacitance by exposure to polar molecules. However, the capacitive LA sensor with a flat-structured PhB/polyvinylchloride (PVC) composite-sensing medium is observed to have a problem in that sensing capacitance variation saturate quickly with increasing the LA solution concentration. This main cause can be analyzed that the interaction of proton from LA molecule with the lone pair electrons of the PhB molecule acts as a major factor on the sensing characteristics rather than the solvatochromic behavior of PhB molecule. Therefore, a strategy is adopted to introduce a porous structure to the PhB/PVC composite-sensing medium to maximize the interaction of PhB with protons, which is implemented through solvent and non-solvent exchange methods. Consequently, the sensitivity and linearity of the porous-structured LA sensor are 2.99 pF mM^{-1} and 0.966 over LA concentrations ranging from 0 to 100 mM, respectively, which is a significant improvement over that of the flat-structured one. Notably, the sensing performance remained unchanged even after a month of storage under normal ambient conditions.

1. Introduction

Organic active materials are gaining extensive attention in various fields of flexible wearable electronic devices,[1–3] including radio-frequency identification tags,[4,5] flexible displays,[6,7] and physical/chemical sensors owing to their advantages such as mechanical flexibility,[8–10] easy molecular design,[11–13] and solution processing.[14–16] Among various application fields, organic physical and chemical sensors are core elements of wearable devices for collecting information of biomechanical and physiological data to diagnose a human disease or monitoring exercise status. A representative indicator for monitoring health status is L-lactic acid (LA) concentration in blood or sweat. LA is an indicator of metabolic disorder status under anaerobic conditions and provides useful information on various diseases or symptoms, such as tissue hypoxia, sepsis, acute heart disease, and metabolic acidosis, as well as exercise training status.[17,18] In addition, as the LA concentration in blood is reflected in the LA concentration of sweat, LA can be profiled indirectly through a non-invasive method.[19] Therefore, various types of organic chemical sensors, which can detect LA concentrations, have been developed such as electrochemical,[20] optical,[21] impedance,[22] capacitive,[23] and transistor-structured applications.[24]

One of the strategies for developing electrochemical LA sensors is to use enzymes for LA molecule recognition.[20] L-lactate oxidase as a representative enzyme oxidizes L-lactate to pyruvate through the flavin mononucleotide reduction in the reduction half-reaction, and oxygen or artificial substance acts as an electron acceptor to re-oxidize the flavin mononucleotide to generate hydrogen peroxide in the oxidation half-reaction.[25] Hydrogen peroxide is detectable through a platinum electrode or a sensing medium such as Prussian blue.[26,27] The method using the enzymes has good selectivity and a high sensitivity for LA; however, it has limitations owing to low biological stability at room temperature and high manufacturing cost.[28] Therefore, to overcome these limitations, the study of non-enzymatic LA sensors is becoming increasingly important.[29–33]

J. Seo, T. Hwang, E. Ko, S. Oh, D. Tsogbayar, Md R. R. Khan, H. S. Lee
Department of Materials Science and Chemical Engineering
Hanyang University
Ansan 15588, Republic of Korea
E-mail: hslee78@hanyang.ac.kr
J. Seo, T. Hwang, S. Oh, D. Tsogbayar, H. S. Lee
BK21 FOUR ERICA-ACE Center
Hanyang University
55 Hanyangdaehak-ro, Sangnok-gu, Ansan 15588, Republic of Korea
J. H. Cho
Department of Chemical and Biomolecular Engineering
Yonsei University
Seoul 03722, Republic of Korea
Y. D. Park
Department of Energy and Chemical Engineering
Incheon National University
Incheon 22012, Republic of Korea
E-mail: ydpark@inu.ac.kr
The ORCID identification number(s) for the author(s) of this article can be found under https://doi.org/10.1002/adfm.202211253.

DOI: 10.1002/adfm.202211253

© 2022 Wiley-VCH GmbH

16163028, 2023, 2, Downloaded from https://onlinelibrary.wiley.com/doi/10.1002/adfm.202211253 by Incheon National University, Wiley Online Library on [10/04/2023]. See the Terms and Conditions (https://onlinelibrary.wiley.com/terms-and-conditions) on Wiley Online Library for rules of use; OA articles are governed by the applicable Creative Commons License

Previously, we reported the LA-chemical sensor system using the solvatochromic behavior of a Nile red (NR, 9-diethylamino-5-benzo[a]phenoxazinone) can solve the problems of having enzyme-based sensors.[23] The solvatochromic behavior is characterized by a change in the bandgap energy according to the polarity of the surrounding molecules, which in turn changes the capacitance (C) of the solvatochromic material. This LA sensor is fabricated through a simple process of coating a composite film of NR and poly(vinyl chloride) (PVC) on an interdigitated electrode (IDE). When the NR/PVC composite-sensing layer is exposed to LA, the C change is translated to a shift in the output phase by the circuit connected to the sensor, which allows the LA concentrations to be detected. The solvatochromism-based LA sensor showed excellent sensing linearity of 0.998, which was interpreted by correlating with the solvatochromic effect and twisted intramolecular charge transfer (TICT) behavior of NR to understand the operating principle of the sensor.[34] However, as a follow-up study was conducted, it was confirmed that there is a limit to fully understand the LA-sensing characteristics caused by these effects. For example, when Phenol blue (PhB, *N*,N-dimethylindoaniline) having solvatochromic property similar to that of NR was applied,[35] a bathochromic shift in which the C increased with exposure to various solvents with increased polarities, whereas the PhB showed hypsochromic shift indicating a decrease in the C exposed with LA solution in reality. These phenomena, as mentioned above, indicate the mechanism alone of detecting LA by solvatochromic and ICT behaviors is insufficient to understand the operating principle of the sensor.

Herein, PhB is a candidate for the expansion of solvatochromic materials capable of detecting LA and a capacitive LA sensor was prepared by applying PhB/PVC composite sensing medium on IDE. PhB shows a bathochromic shift in which absorption maxima increases in a polar solvent environment, such as NR, which is suitable for use as a sensing probe in an aqueous environment such as a LA solution owing to low solubility in water. In this study, various spectroscopic analyses of the solutions containing PhB and LA were performed to analyze the interaction between PhB and LA, and a comparative study was conducted to elucidate the sensing principle of the PhB/PVC-sensing medium. Based on the results, we proposed an additional LA sensing mechanism along with the solvatochromic and ICT behaviors in PhB/PVC composite sensing medium. According to the proposed mechanism, the sensing performance was greatly improved by controlling the morphology of the PhB/PVC-sensing medium in the sensor, which has led to developing a capacitive LA sensor with excellent sensitivity, linearity, and reliability in the sensing performances.

2. Result and Discussion

To confirm the potentials of PhB as a solvatochromic-based LA sensing probe, we first simulated the molecular orbital structures and their energy levels of a gas-phase PhB visualized through density functional theory (DFT) calculation with the approach of polar molecule. According to the DFT calculation results, the imine group of PhB molecule was twisted during the ICT process in which the charge was transferred from the dimethylamine group to the ketone group.[35–40] The planar state and twisted state resulted in the ICT behavior of PhB molecules are determined by the electrostatic repulsion in the molecule and the molecular-molecular interaction, which causes the polarity change of the PhB molecule. In particular, a molecule with an electron-donating group capable of molecular geometry rotation, such as the dimethylamine group of PhB, could convert a twisted state. Owing to this ICT behavior, the band gap energy was 2.69 eV when the molecular structure is planar state, whereas the band gap energy was reduced to 2.50 eV in the twisted state. Therefore, the PhB sensing probe is expected to present a bathochromic shift as the polarity of solvent increases and the bandgap energy decreases with the TICT behavior, resulting in the increase of C.[35–41] **Figure 1b** shows the ultraviolet-visible (UV-vis) spectroscopic results of 40 μM PhB solutions in various solvents to confirm the TICT characteristics of PhB molecules with the solvent polarity.[35–39] The absorption maxima (λ_{max}^{abs}) of various PhB solutions were observed at 551 nm for cyclohexane (CH), 570 nm for toluene (Tol), 589 nm for dichloromethane (DCM), 594 nm for N,N-dimethylacetamide (DMAC), 593 nm for N,N-dimethylformaide (DMF), 606 nm for dimethyl sulfoxide (DMSO), 605 nm for ethanol (EtOH), and 659 nm for the mixed solvent of 10 vol% EtOH and deionized (DI) water. The λ_{max}^{abs} changes of the PhB solutions with various solvents can be seen in an obvious trend when compared with the Reichardt polarity function ($E_T(30)$) shown in Table S1 (Supporting Information), which represents the degree of polarity. Figure 1c demonstrated the variations of the λ_{max}^{abs} values as a function of $E_T(30)$ and a proportional relationship with considerable linearity between the two was observed. As expected from the DFT calculations, as the polarity of the solvent molecules increases, the λ_{max}^{abs} of the PhB solution shows a bathochromic shift moving to the up-shift direction, and this behavior of the PhB molecules suggests the potential as a sensing probe capable of detecting the polar LA molecules. Actually, the PhB solution is purple when dissolved in the nonpolar CH and blue when dissolved in the polar EtOH as shown in Figure S2 (Supporting Information). These color changes were consistent with the variations in λ_{max}^{abs} values. More detailed information of λ_{max}^{abs} and $E_T(30)$ is summarized in Table S1 (Supporting Information).

The basic hypothesis of our system is that when LA molecules are exposed to the solvatochromic PhB sensing medium, the sensing medium changes the bandgap energy according to the approach of the surrounding polar molecules and the C value changes owing to the interaction between the sensing medium and LA molecules, and this principle can be applied as a chemical sensor capable of detecting LA molecules or concentrations. We constructed a composite with hydrophobic PVC utilizing PhB as a sensing medium for LA detection. This PhB/PVC composite film was coated on IDE to fabricate a capacitive LA sensor, as shown in Figure 1d. (Refer to the Experimental section and Figure S3 (Supporting Information) for detailed device preparation process). In Figure 1f,g, the prepared PhB/PVC film surface was confirmed to have a flat morphology with *rms* roughness of ≈1.19 nm and its σ value was obtained based on the Gaussian fitting of the height histogram and calculated as 1.058 nm with superior roughness uniformity. The low *rms* roughness and morphological uniformity contribute to

 © 2022 Wiley-VCH GmbH

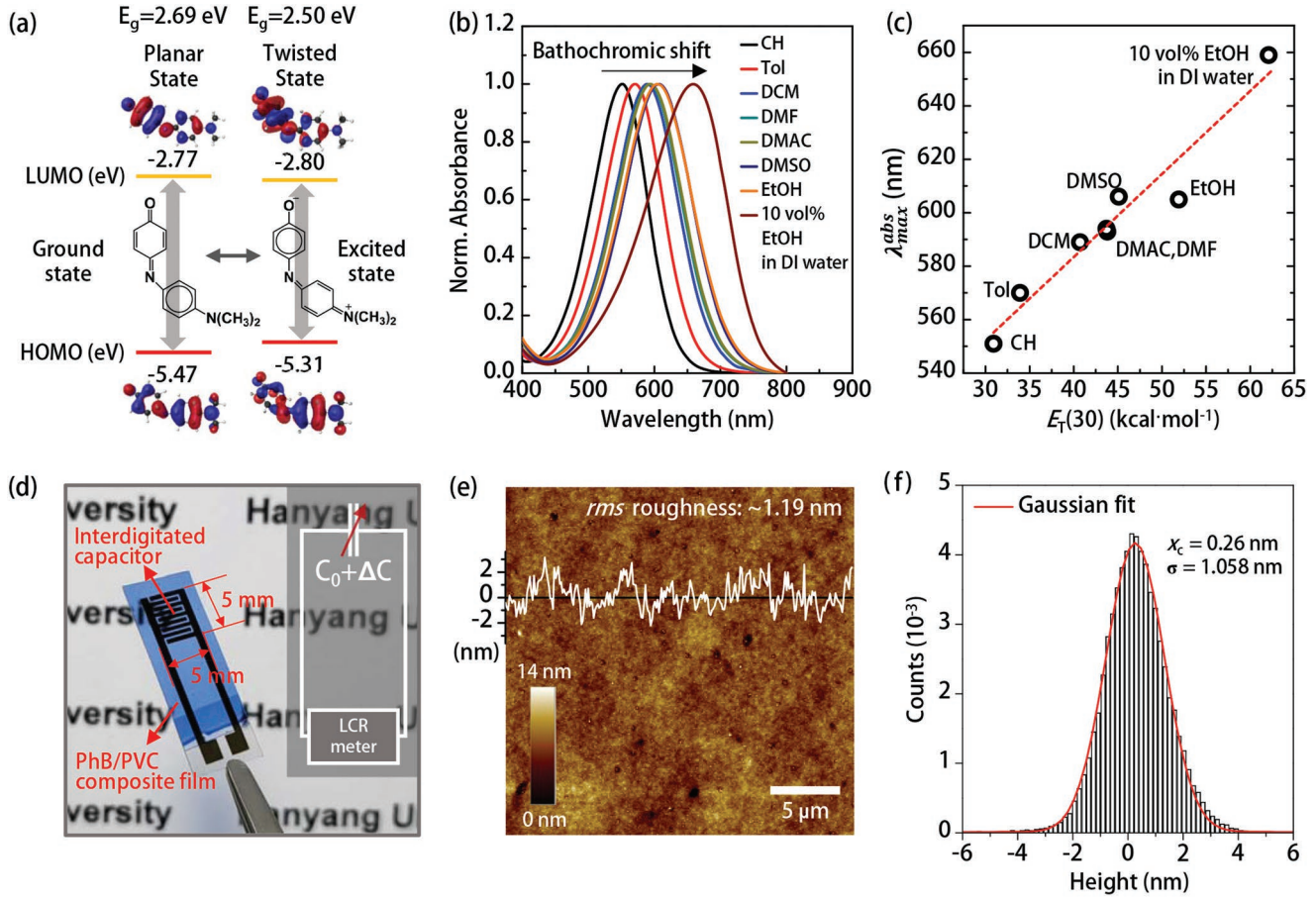

Figure 1. a–c) Structural and spectroscopic analysis of solvatochromic behavior of PhB molecules. a) The schematic diagram representing the calculation of the difference in molecular orbital structure of PhB molecules according to conformational change and ICT behavior of the PhB molecule using the DFT function. b) UV–vis spectroscopic results of PhB solution using various solvents and c) The absorption maxima of b) sorted according to E_T(30). d–f) A capacitive sensor based on a PhB/PVC composite film as a sensing layer. d) The photograph and the brief circuit diagram of the PhB-sensor. e) AFM image and height profile of the surface of the PhB/PVC composite film. f) Histogram of height distribution function based on e).

the transparent properties of the PhB/PVC composite sensing medium shown in Figure 1d.

Figure 2 shows the sensing performance characteristics of our capacitive LA sensor with the PhB/PVC composite sensing medium for aqueous LA solutions with various concentrations from 0 to 100 mM. Hereinafter, the LA sensor with PhB/PVC composite sensing medium will be referred as PhB-sensor. During this experiment, while applying AC voltage of 1 V and 10 kHz to the PhB-sensor, the LA solutions were injected onto the sensing area and then removed at regular intervals to test the LA sensing characteristics. A schematic diagram of such analysis system is shown in Figure S4 (Supporting Information). As shown in Figure 2a, the PhB-sensor shows stable repeatability with respect to exposure to the LA solutions, with an increase in C value upon exposure to an LA solution and a decrease in C value upon removal of the solution. These results could be explained by the TICT behavior that occurs when the PhB molecules are exposed to the polar LA solution, as described in our previous study,[23] inducing the decrease in the bandgap energy and the increase in C of the sensing medium.

Figure 2b–d and Table S2 (Supporting Information) summarize the results obtained from measuring five other devices prepared by the same process. The C values of the PhB-sensors were measured to be 4.74 ± 0.10 pF in air and 21.9 ± 0.12 pF in DI water, confirming that the C of the PhB sensor increased even when exposed to DI water. This is because of two reasons, one is that the DI water itself interposed between the IDEs and acted as an additional capacitor, and the other is that the high polarity of water molecules induces polarization in the sensing medium, which could be related to increase in C.[42] The PhB-sensors exposed to 0.01 mM LA solution showed C variations of 21.3 ± 0.24 pF, almost similar to those of DI water exposure. However, with the increase in concentrations of the LA solutions to 0.1, 1.0, and 5.0 mM, the C values increased to 35.5 ± 0.63, 139.2 ± 2.01, and 214.3 ± 3.86 pF, respectively, which confirmed a somewhat constant trend in C variations. These trends can be confirmed in a graph in which the LA concentration change is expressed on a log-scale as shown in Figure 2b. However, the most serious drawback of our PhB-sensor is that the sensing signal saturates too quickly as the LA concentration increases. In fact, the variation in C values does not show any meaningful results in the section over the concentration of 5 mM. In addition, the sensitivities and linearities were 37.0 pF mM^{-1} and 0.790 or 0.168 pF mM^{-1} and 0.628,

© 2022 Wiley-VCH GmbH

16163028, 2023, 2, Downloaded from https://onlinelibrary.wiley.com/doi/10.1002/adfm.202211253 by Incheon National University, Wiley Online Library on [10/04/2023]. See the Terms and Conditions (https://onlinelibrary.wiley.com/terms-and-conditions) on Wiley Online Library for rules of use; OA articles are governed by the applicable Creative Commons License

16163028, 2023, 2, Downloaded from https://onlinelibrary.wiley.com/doi/10.1002/adfm.202211253 by Incheon National University, Wiley Online Library on [10/04/2023]. See the Terms and Conditions (https://onlinelibrary.wiley.com/terms-and-conditions) on Wiley Online Library for rules of use; OA articles are governed by the applicable Creative Commons License

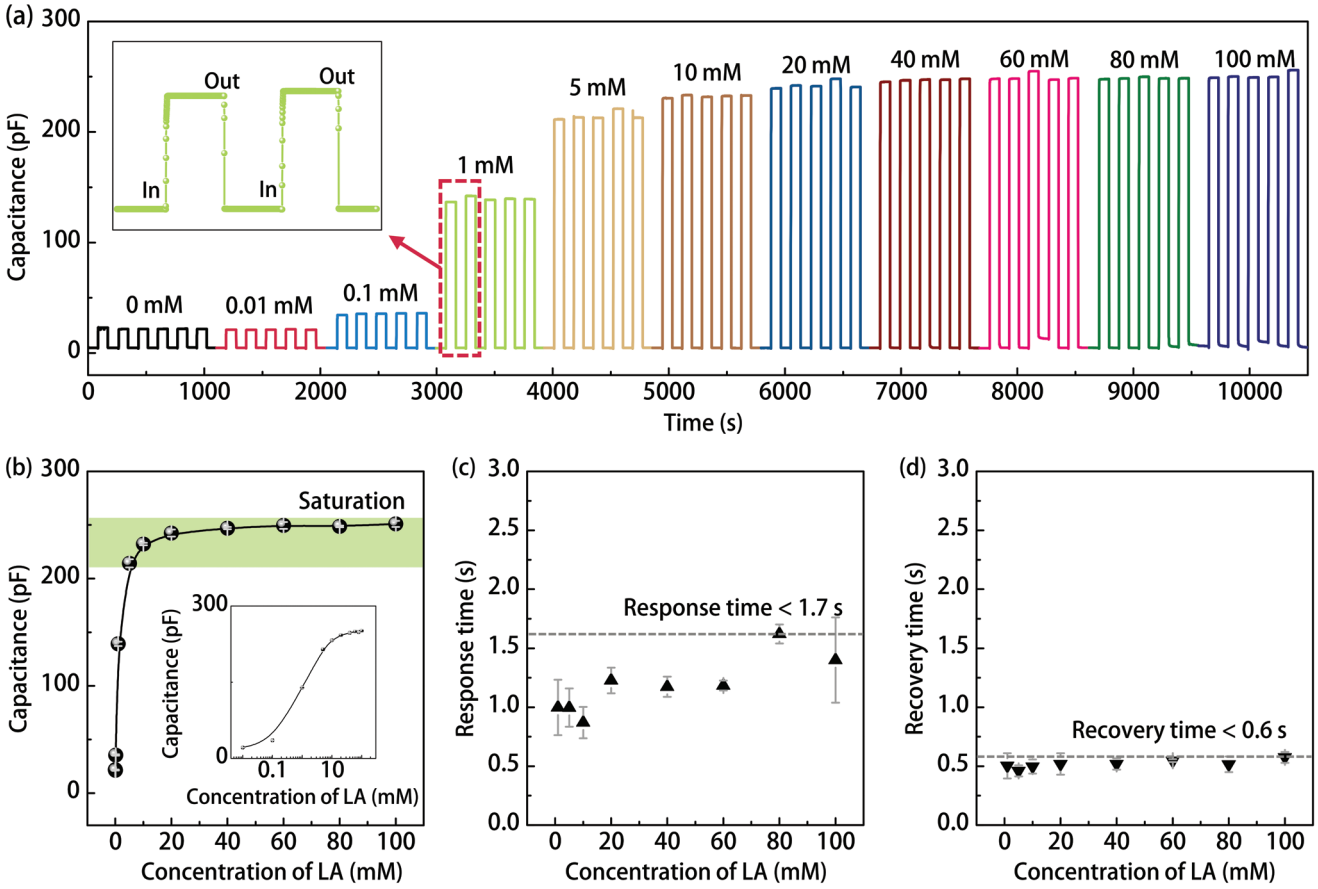

Figure 2. Performance characteristics of PhB-sensors a) Capacitance as a function of the time of the PhB-sensor exposed to various 0 to 100 mM LA aqueous solutions. b) Capacitance variation as a function of concentration of LA from 0 to 100 mM. This plot had the saturated response region. Inset plot: *x*-axis of log scale. (n = 5) c) Response time variations as a function of concentration of LA from 0 to 100 mM. (n = 5) d) Recovery time variations as a function of the concentration of LA from 0 to 100 mM. (n = 5)

respectively, in the sections of 0 ~ 5 mM or the 10 ~ 100 mM LA concentrations, indicating very low sensing reliability as a sensor performance, shown in Figure S5 (Supporting Information). On the other hand, the response and recovery times of the PhB-sensor showed excellent results of less than 1.7 and 0.6 s, respectively, in all concentration sections. (See Figure S6, Supporting Information for the definitions used to calculate the response and recovery times). Consequently, we confirmed the applicability of the PhB/PVC composite sensing medium as a probe for LA detection by repeatedly increasing the C when the PhB-sensors were exposed to an LA solution. However, the rapid sensing signal saturation and nonlinearity in the C values according to the LA concentration were identified as the thresholds to be overcome for applying as a sensor. Therefore, it is necessary to address these issues by more precisely investigating the interaction between PhB and LA molecules and understanding the mechanism to detect the LA molecules in the PhB-sensor.

To better understand the interaction between PhB and LA molecules, we performed spectroscopic analyses and inferred interesting facts from the obtained results. **Figure 3a** shows the results of UV-vis spectroscopy analyzed by adding various concentrations of LA solutions from 0 to 100 mM into 10 vol% EtOH aqueous solution containing 40 μM PhB. The λ_{max}^{abs} s of the PhB solution were the same at 659 nm for 0 and 0.01 mM LA, but showed a hypsochromic shift tendency to 586 nm at 0.1 mM LA and 568 nm at 1, 10, and 100 mM LA. This tendency suggests that the PhB molecules were in the twisted state at low-concentrated LA solution of 0 or 0.01 mM and in the planar state at high-concentrated LA solution of greater than 1 mM. This result is contrary to the bathochromic shift caused by the TICT behavior previously described as a mechanism through which PhB/PVC-sensing medium in the PhB-sensor detects the LA molecules. In other words, the PhB molecule exhibits the TICT behavior owing to the solvatochromic effect induced by the surrounding polar molecule is confirmed; however, it is unable to fully explain the working principle of our sensor for the LA detection. Especially, considering the dissociation process of a LA molecule in aqueous phase, a LA molecule is ionized into proton and lactate. Therefore, we need to confirm which one of them interacts dominantly with the PhB molecules. To determine whether the proton or lactate interacts significantly with the PhB molecule, we prepared a system that simulated the pH with concentrations of LA solutions using HCl solution. Figure 3b shows the results of UV-vis spectroscopy when the pH-adjusted HCl solutions were added

 © 2022 Wiley-VCH GmbH

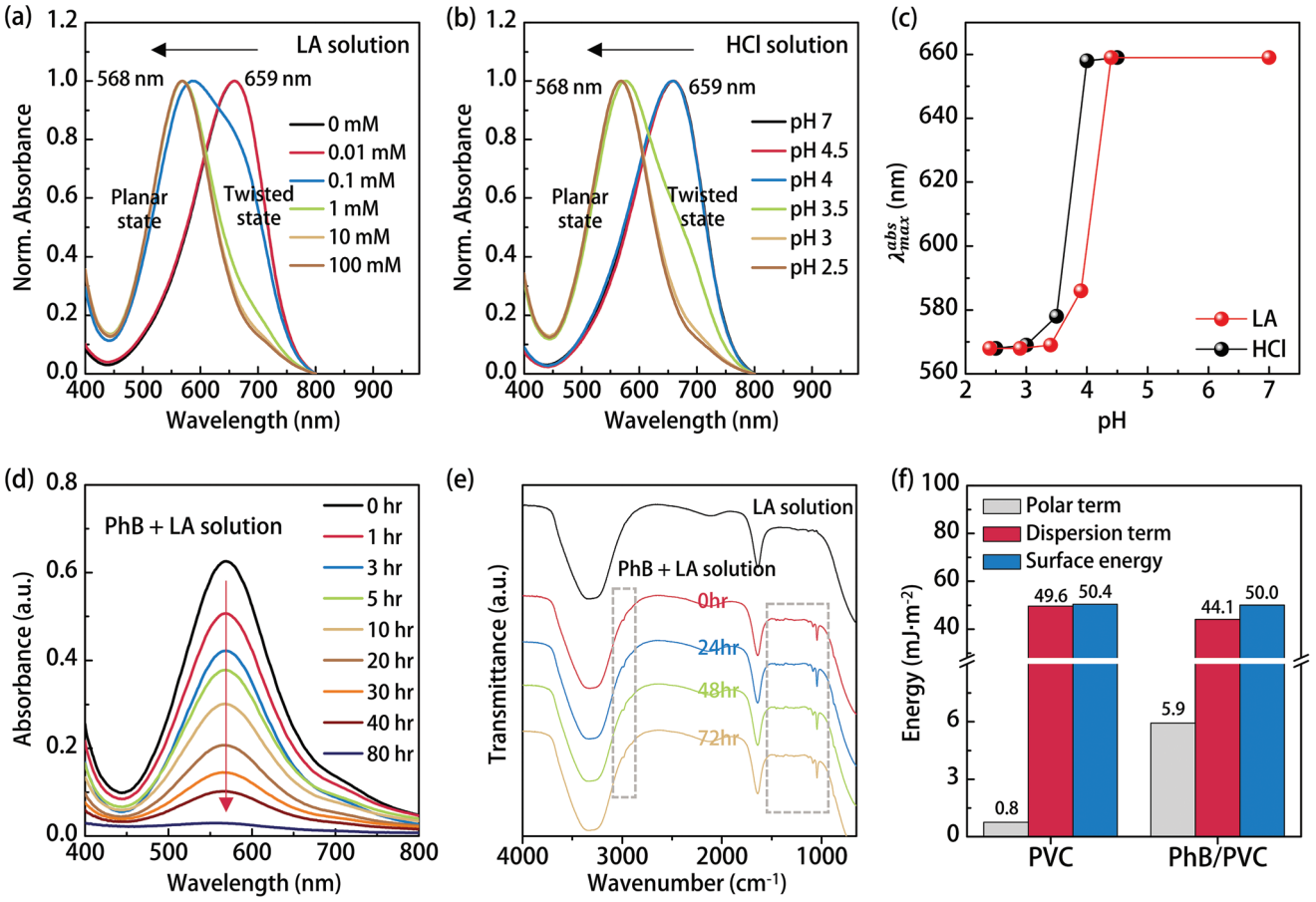

Figure 3. a–e) Spectroscopic analysis to understand the interaction between PhB and LA a) UV-vis spectroscopic results of 10 vol% EtOH solution containing 0 to 100 mM LA and 40 μM PhB. b) UV-vis spectroscopic results of 10 vol% EtOH solution containing 40 μM PhB and pH adjusted using HCl c) λ_{max}^{abs} in a,b) plots sorted according to the pH of the solution. d,e) After preparing a 10 vol% solution of EtOH containing 100 mM LA and 40 μM PhB. d) UV-vis spectroscopic results from 0 to 80 h. e) FT-IR spectroscopic results from 0 to 72 h. f) Summary of the surface energy, polar term, and dispersion term for the surface of a PVC film and a PhB/PVC composite film.

to 10 vol% EtOH solution containing 40 μM PhB. As shown in the figure, the λ_{max}^{abs} s were observed at 659 nm for the cases of pH 7 ~ 4 range, 578 nm for the pH 3.5 case, and 568 nm for the cases of pH 3 and 2.5. Figure 3c is a result to clearly compare the λ_{max}^{abs} variations shown in Figure 3a,b, showing almost similar peak-shifting tendency, although not perfectly matched. In other words, we could expect that the PhB acts as a sensing medium owing to the elements that LA and HCl solutions have in common. Based on this comparison, the PhB molecule are expected to interact mainly with the protons rather than lactate, causing TICT behavior from the twisted to planar states, because the PhB molecules cannot interact with negative ions due to repulsive interaction. Therefore, these results could be interpreted as being caused by the electrostatic interaction between the protons and the lone pair electrons in the ketone or imine groups of the PhB molecule.[43–45]

In addition, to check whether the interaction between PhB and LA molecules varies with time, a 10 vol% EtOH aqueous solution containing a relative high concentration of 100 mM LA and 40 μM PhB was stored for a long time of 80 h, and UV-vis spectrum analysis was performed over time. As a result, the absorbance of the solution decreases over time, suggesting that the interaction between PhB and protons inhibits the ICT behavior of the PhB molecules.[35,42] The color change in the solutions when stored at 4 °C for 80 h after mixing LA solutions of various concentrations with 40 μM PhB solution is shown in Figure S7 (Supporting Information). To confirm whether these changes in the absorbance of UV-vis spectrum is a phenomenon caused by the chemical reaction (or interaction) between the LA and PhB molecules, Fourier transform infrared (FT-IR) spectroscopic analyzes were performed after 0, 24, 48, and 72 hrs by preparing the 100 mM LA solutions containing 40 μM PhB shown in Figure 3e. As seen from the figure, the transmittances did not change with time, which leads to the conclusion that the chemical reaction (or interaction) between the PhB and LA molecules is not the reason for the variations presented in Figure 3(a–d). Therefore, the conclusion from these analyses is that the LA detection mechanism of the PhB-sensor with PhB/PVC composite sensing medium is mainly owing to the interaction of the PhB molecule with protons and not the TICT behavior of the PhB molecules.

The spectroscopic analyses of the interaction between PhB and LA in the solution state were not a system consistent with the solid-state PhB/PVC composite-sensing medium proposed

© 2022 Wiley-VCH GmbH

16163028, 2023, 2, Downloaded from https://onlinelibrary.wiley.com/doi/10.1002/adfm.202211253 by Incheon National University, Wiley Online Library on [10/04/2023]. See the Terms and Conditions (https://onlinelibrary.wiley.com/terms-and-conditions) on Wiley Online Library for rules of use; OA articles are governed by the applicable Creative Commons License

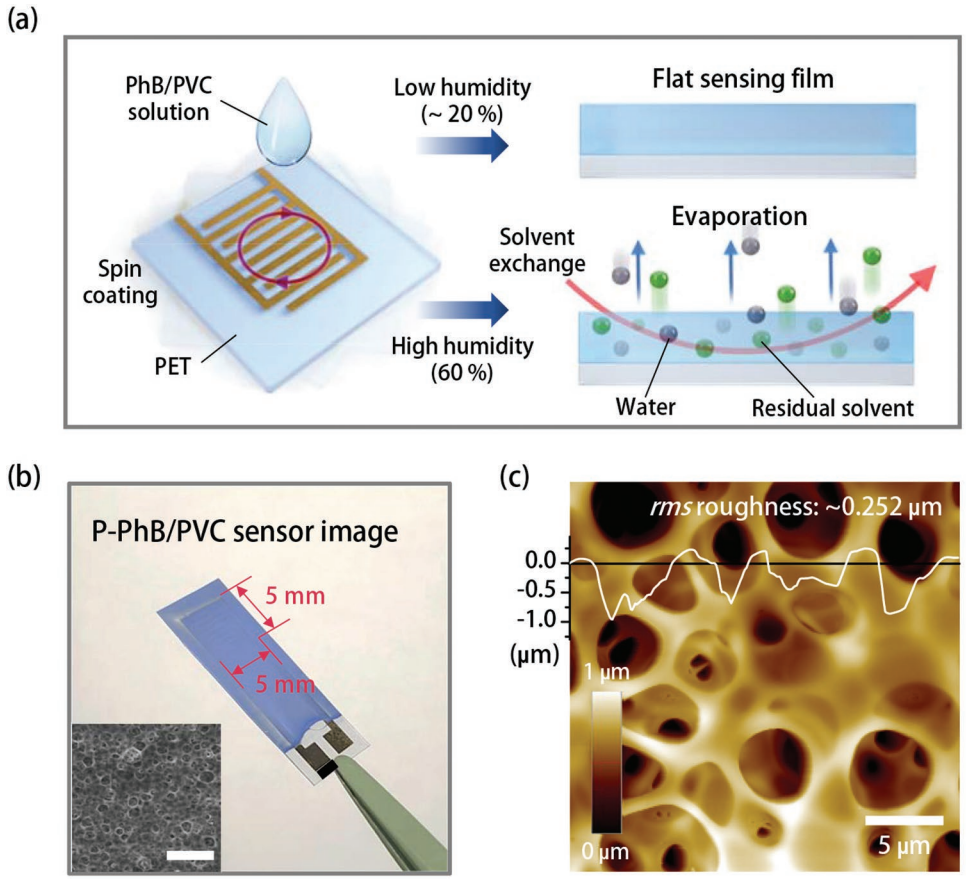

Figure 4. The *p*-PhB/PVC composite film fabricated by solvent exchange method. a) Schematic diagram of the fabrication process and porous structure formation mechanism of *p*-PhB/PVC composite film. b) A photograph of the *p*-PhB-sensor. Inset is SEM image of the surface of the *p*-PhB/PVC composite film (scale bar = 20 μm) c) AFM image and height profile of the surface of the *p*-PhB/PVC composite film.

in this study. Thus, UV–vis spectroscopic analysis was performed following exposure of various concentrations of LA solution to solid-state PhB/PVC composite film as shown in Figure S8 (Supporting Information). No spectroscopic change, however, was observed in the PhB/PVC composite films, therefore, there is a limit to deriving a meaningful interpretation from these analyses. By comparing the surface energies of PVC only and PhB/PVC composite films, we were able to infer the effect of the LA on the PhB/PVC composite sensing layer. As shown in Figure 3f, the surface energies of the PVC only and PhB/PVC composite films were similar to 50.4 and 50.0 mJ m^{-2}, respectively, but the polar term dramatically increased from 0.8 to 5.9 mJ m^{-2}. The increase in the polar term is due to the exposed PhB on the surface of PhB/PVC composite film, where a strong interaction occurs between the exposed PhB and protons from the LA molecule. Therefore, the C value of the PhB-sensor increases with exposure to the LA solution mainly because of the adsorption of protons to PhB molecules on the surface of the sensing medium, inducing the polarization of PhB/PVC composite-sensing medium.[42,46] Based on these results, we can hypothesize that if the adsorption efficiency of the LA molecules to the PhB/PVC composite-sensing medium is increased, the sensing performances of our PhB-sensor can be dramatically improved by solving problems such as fast signal saturation and low linearity shown in Figure 2.

Based from the above results, a strategy was devised to improve the specific surface area of the PhB/PVC composite-sensing medium for maximizing the effective interfacial area between PhB and LA molecules. **Figure 4a** shows a schematic diagram of the solvent and non-solvent exchange method for implementing the porous PhB/PVC (*p*-PhB/PVC) composite-sensing medium. The aforementioned flat PhB/PVC composite-sensing medium was prepared in a low-humidity environment of ≈20%. Whereas, when the film is dried in a high humidity condition of ≈60%, the DMAC solvent vapor in the film is exchanged with water, which is a non-solvent vapor, thereby inducing the formation of a porous structure in the PhB/PVC film.[47,48] Figure 4b,c show the images of the *p*-PhB/PVC composite film prepared by this method by analyzing SEM and AFM, respectively, which is opaque unlike the flat PhB/PVC composite film shown in Figure 1d. As shown in the figures, numerous pores are observed to be formed on the surface with diameters of 3.8 ± 0.9 μm (n = 50) and depths of 7.0 ± 0.2 μm (n = 20). In particular, such porous structures were formed not only on the surface of the *p*-PhB/PVC composite film but also on the bulk region as shown in Figure 4(c), confirming that it is an effective approach that can dramatically improve the interfacial area where PhB and LA molecules interact.

Figure 5 demonstrates the sensing characteristics of the capacitive LA sensor with the *p*-PhB/PVC composite-sensing

© 2022 Wiley-VCH GmbH

16163028, 2023, 2, Downloaded from https://onlinelibrary.wiley.com/doi/10.1002/adfm.202211253 by Incheon National University, Wiley Online Library on [10/04/2023]. See the Terms and Conditions (https://onlinelibrary.wiley.com/terms-and-conditions) on Wiley Online Library for rules of use; OA articles are governed by the applicable Creative Commons License

16163028, 2023, 2, Downloaded from https://onlinelibrary.wiley.com/doi/10.1002/adfm.202211253 by Incheon National University, Wiley Online Library on [10/04/2023]. See the Terms and Conditions (https://onlinelibrary.wiley.com/terms-and-conditions) on Wiley Online Library for rules of use; OA articles are governed by the applicable Creative Commons License

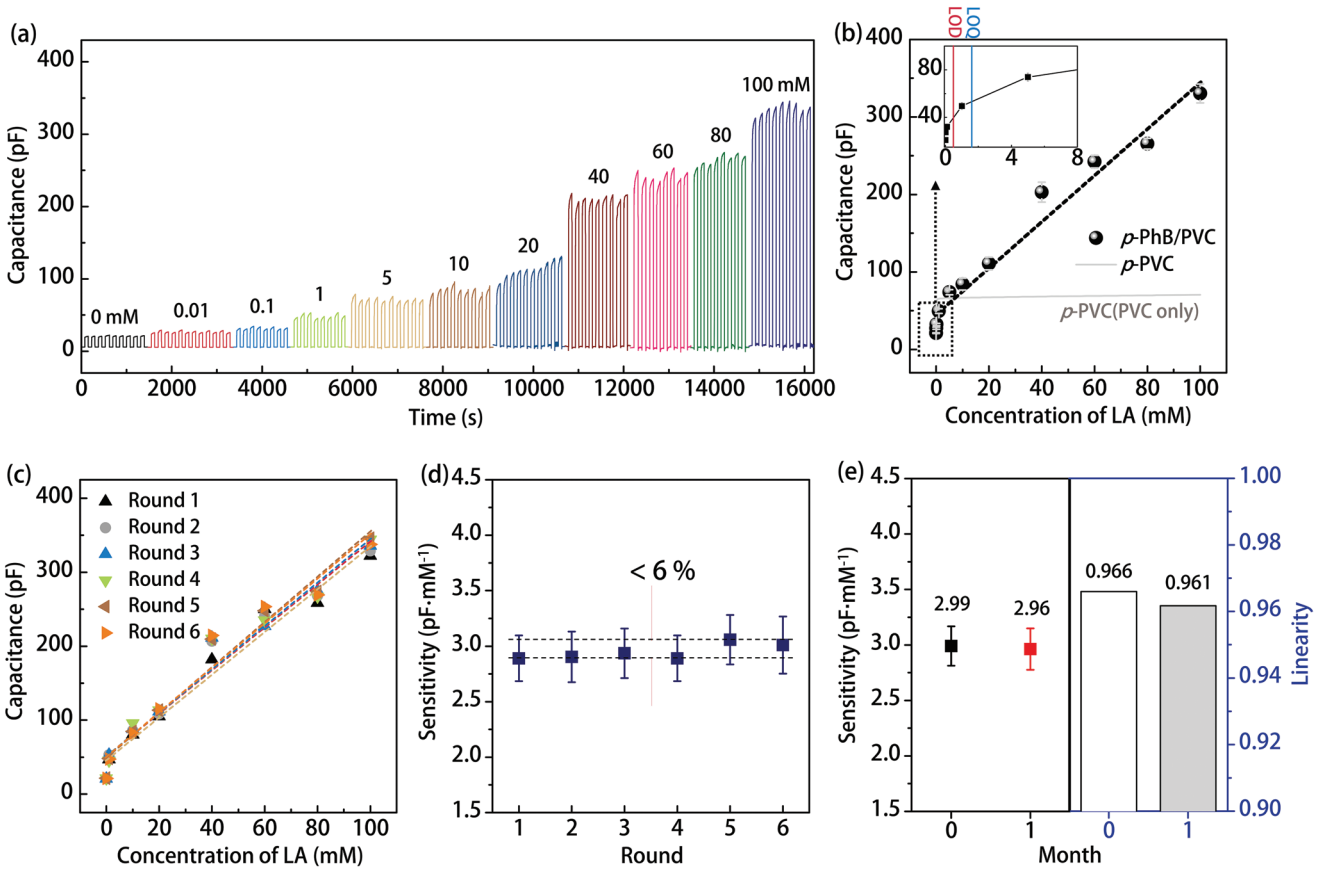

Figure 5. Performance characteristics of *p*-PhB-sensors a) Capacitance as a function of time of the *p*-PhB-sensor exposed to various 0 to 100 mM LA aqueous solutions. b) Capacitance variations as a function of the concentration of LA from 0 to 100 mM. Inset plot: 0 to 8 mM LA region magnification. (n = 8) c,d) After repeated exposure to 0 to 100 mM LA aqueous solution up to round 6, c) The capacitance and d) Sensitivity of the *p*-PhB-sensor in each round. e) Summary of sensitivity and linearity of the *p*-PhB-sensor stored in ambient atmosphere for a month.

medium for aqueous LA solution with various concentrations from 0 to 100 mM. Hereinafter, the LA sensor with *p*-PhB/PVC composite sensing medium will be referred to as *p*-PhB-sensor. The C values are confirmed to repeatedly and reliably change in the *p*-PhB-sensor as it is exposed to various concentrations of LA solution, such as the flat PhB-sensor shown in Figure 2, although degree of change in C values varies to some extent in Figure 5a. In particular, the most striking difference between the *p*-PhB- and PhB-sensors is that the saturation problem does not appear even in the section with an LA concentration of 5 mM or higher. Figure 5b shows the results of summarizing the average Cs and their standard deviation for 8 samples, and the detailed values are summarized in Table S3 (Supporting Information). The sensing performances of the *p*-PhB-sensor from 0 to 100 mM LA aqueous solutions were calculated with a sensitivity of 2.99 pF mM^{-1} and a linearity of 0.966, which were a dramatic improvement compared to that of the PhB-sensor cases. However, the porous PVC-only film does not show any response to exposure to LA solutions. (Gray line in Figure 5b) These results could be attributed to the increase in surface exposure of PhB molecules and the contact efficiency of LA molecules owing to the porous structure of the *p*-PhB/PVA composite-sensing medium, suggesting that our strategy effectively improves the LA-sensing performance and addresses the signal saturation problem in the capacitive LA *p*-PhB-sensor. However, although the performance of the *p*-PhB-sensor was improved compared to that of the PhB-sensor, some problems were still identified. A representative problem among these was the lack in discrimination of the sensing characteristics in a low concentration LA solution of less than 1 mM. As shown in Figure 5a,b, no significant difference was found in the C variation between exposure to pure DI water and 0.01 or 0.1 mM LA solutions. Therefore, we calculated the limit of detection (LOD) and limit of quantitation (LOQ) based on the results of Figure 5b, which were 0.49 and 1.61 mM, respectively. (Refer Figure S9, Supporting Information). These LOD and LOQ were obtained by the equation below,[49]

$$\mathrm{LOD} = \frac{3 \times \text{standard deviation at 0m MLA}[\mathrm{pF}]}{\text{sensitivity}\left[\mathrm{pF \cdot mM^{-1}}\right]}, \qquad \mathrm{LOQ} = 3.3 \times \mathrm{LOD} = 3.3 \times \mathrm{LOD} \tag{1}$$

The target application fields of our sensor are the wearable sensory systems that can be attached to the skin to evaluate the degree of fatiguability through the detection of LA concentration in the sweat. In general, human sweat contains ≈4 to 25 mM of LA concentration in a stable state and more than

 © 2022 Wiley-VCH GmbH

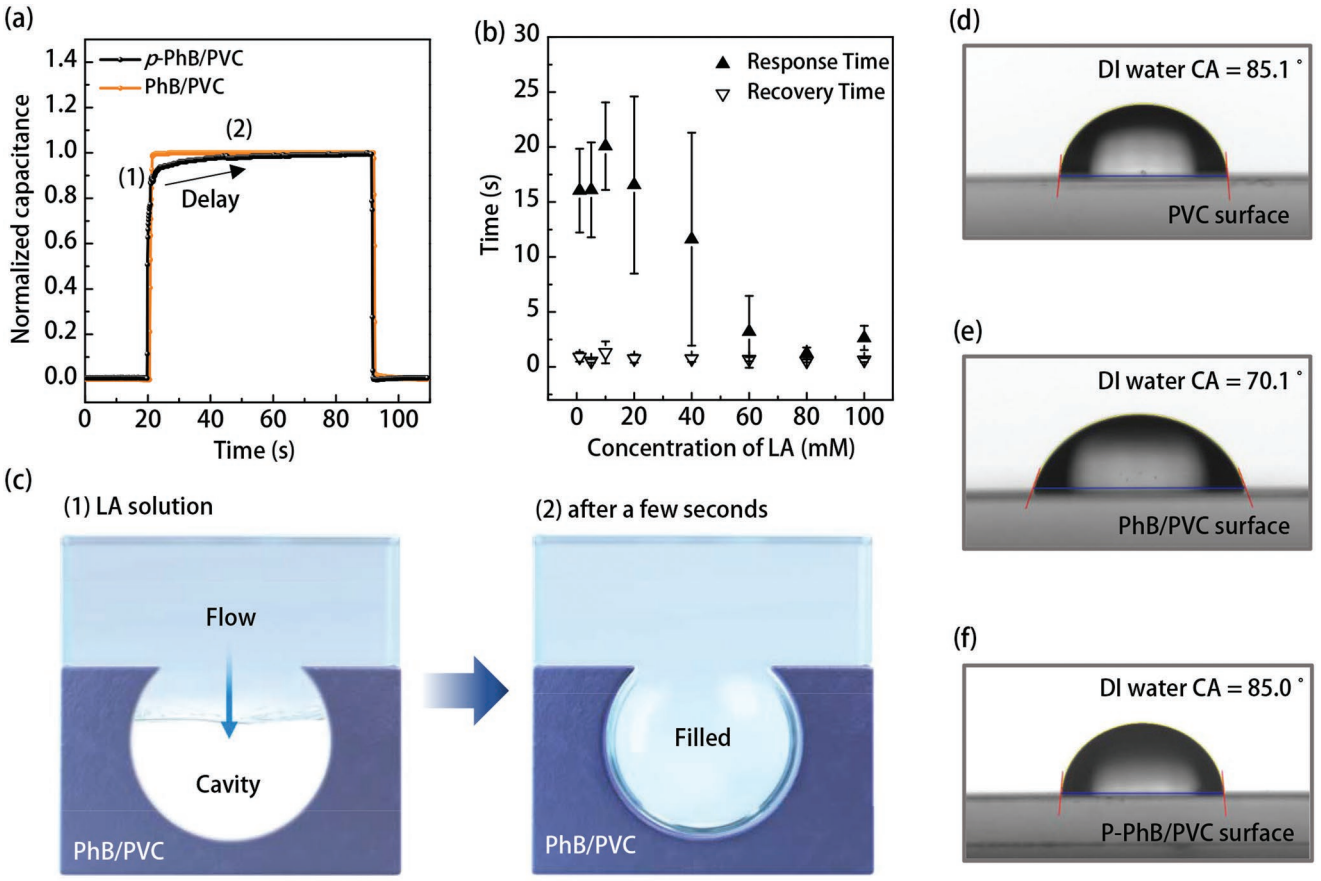

Figure 6. a) Difference in capacitance with time in *p*-PhB- and PhB-sensors when exposed to 60 mM LA b) Response and recovery time variations as a function of LA concentration from 0 to 100 mM. c) Schematic diagram of the mechanism by which signal delay occurs in the *p*-PhB-sensor. d–f) CA comparison of DI water on each surface d) a PVC film, e) a PhB/PVC film, f) a *p*-PhB/PVC composite film.

50 mM LA concentration during intense exercise state.[27] Therefore, the LOD and LOQ of the developed capacitive LA *p*-PhB-sensor is considered to be at a level that does not interfere with application of a skin-attachable sensory device. In addition, the sensitivity and linearity of *p*-PhB-sensors excluding the LOD range below 0.49 mM are calculated as 2.77 pF mM^{-1} and 0.972, respectively, which are excellent sensing performances for LA detection.

To evaluate the reliable stability of the *p*-PhB-sensor developed in this study, we measured the variations in C value when one device was repeatedly exposed six times to an LA aqueous solution at a concentration of 0 to 100 mM. As shown in Figure 5c, the C value changes were approximately similar for the six repeated measurements and the sensitivities calculated from these results are summarized in Figure 5d. The sensitivity of the *p*-PhB-sensor during six repeated measurements is within 6% of the error range, confirming the excellent stability and reliability of the sensor. Furthermore, as shown in Figure 5e, after being stored for a month under atmospheric conditions to confirm the long-term stability of the sensor, the *p*-PhB-sensor showed a sensitivity and linearity of 2.96 pF mM^{-1} and 0.961, respectively, showing changes within the error ranges of 1% and 0.5%, respectively. These results verify that the capacitive LA *p*-PhB-sensor introduced in this study has sufficiently secured a sensitivity, reliability, and stability for the LA detection. Therefore, it can be proposed as a biosignal-detectable sensor applicable to wearable sensor systems in future.

Another problem with the aforementioned *p*-PhB-sensors developed in this study is that the response rate (or time) is delayed when exposed to LA solution. **Figure 6a** representatively shows an enlarged view of a specific section obtained after exposure to LA solution of 60 mM concentration with normalizing one of the signals. By superimposing the signals of the PhB- and *p*-PhB-sensors, the problem for the signal delay is clearly observed. The result of summarizing the response and recovery times of the *p*-PhB-sensor according to each LA concentration is presented in Figure 6b. In addition, the detailed response and recovery times are summarized in Table S3 (Supporting Information). We could infer that the main reason for the delayed response time is that the LA aqueous solution needs time to sufficiently fill the air gaps in the numerous pores formed on the surface of the *p*-PhB/PVC composite-sensing medium as schemed in Figure 6c. This assumption can be supported by the analysis of the surface energy of the sensing medium through the measurement of the contact angle shown in Figure 6d–f. The water contact angle of the PVC-only surface is 85.1°, whereas its angle for the PhB/PVC film surface is reduced to 70.1° owing to the polar PhB molecules. On the

© 2022 Wiley-VCH GmbH

16163028, 2023, 2, Downloaded from https://onlinelibrary.wiley.com/doi/10.1002/adfm.202211253 by Incheon National University, Wiley Online Library on [10/04/2023]. See the Terms and Conditions (https://onlinelibrary.wiley.com/terms-and-conditions) on Wiley Online Library for rules of use; OA articles are governed by the applicable Creative Commons License

other hand, the contact angle for the *p*-PhB/PVC composite film is significantly increased to 85° due to the air trapped in the porous structure on the surface. This increased hydrophobicity of the surface may be the reason the LA aqueous solution takes time to sufficiently wet the *p*-PhB/PVC composite surface.

The significance of our study is that we confirmed that PhB could be used as a probe medium capable of sensing LA, and a strategy was suggested to solve the problems of our previous study of low sensitivity as a capacitive sensor by controlling the film morphology of the sensing medium. In addition, the strategy for improving the sensing characteristics using the porous sensing medium can be applied in various ways to maximize the contact-interfacial area, such as the application of the electrospun nanofiber sensing medium and is expected to greatly help the development of capacitive chemical sensors in the future.

3. Conclusion

In summary, we developed a capacitive sensor using the PhB/PVC composite-sensing medium to strengthen the detection capability of LA. The original purpose of the study was to enhance a capacitive LA sensor performance based on the ICT behavior of PhB molecules in sensing medium to LA exposure. However, this PhB-sensor showed a problem that the sensing signal saturated quickly, such as the sensitivities of high 37.0 pF mM^{-1} and low 0.168 pF mM^{-1} in 0–5 mM and 10 ~ 100 mM LA concentration regions, respectively. These results could be speculated that the solvatochromic behavior of the PhB molecule clearly affects the sensing characteristics of the LA molecule; however, the interaction of proton from LA molecule with the lone pair of electrons of the PhB molecule has a more important effect on the sensing characteristics. Thus, a strategy to solve the signal saturation problem was newly devised as maximizing the effective interfacial area between PhB and LA molecules. Based on this strategy, the PhB/PVC composite-sensing medium was designed with a porous structure using the solvent and non-solvent exchange method to improve the specific surface area of the sensing medium. As a result, the sensitivity and linearity of the *p*-PhB-sensor with porous PhB/PVC composite-sensing medium was 2.99 pF mM^{-1} and 0.966 over the LA concentrations from 0 to 100 mM, respectively, which was significantly improved compared to that of the PhB-sensor. Notably, the sensing performance remains almost the same even after a month of storage under normal ambient conditions. Our achievements are expected to contribute to the development of biosensors with excellent reliability as well as improved characteristics of detecting biosignal substances including lactic acid.

4. Experimental Section

Materials: PhB (97%), CH (anhydrous, 99.5%), Tol (anhydrous, 99.8%), DCM (anhydrous, ≥99.8%), DMAC (spectrophotometric grade, ≥99%), EtOH (200 proof, anhydrous, ≥99.5%), and PVC (High molecular weight) were purchased from Sigma–Aldrich without additional purifications. DMF (special grade, 99.5%), DMSO (extra pure, 99.0%), acetone (99.5%, Extra pure), 2-propanol (99.5%, anhydrous), and HCl (extra pure, 35.0~37.0%) were purchased from Samchun Chemicals. Polyethylene terephthalate (PET) film was purchased from Film-Bank. LA (85%) was purchased from TCI.

Preparation of PhB/PVC Solution: PhB was dissolved in DMAC at a concentration of 5 mg mL^{-1}. To dissolve the PhB solution, the solution was ultrasonicated for 15 min at room temperature. Then, 100 mg mL^{-1} PVC was added to the prepared PhB solution and stirred at 60 °C for 15 h. After the PhB and PVC were completely dissolved, the solution was left stirring until room temperature.

Fabrication of Capacitive LA Sensors: A188 µm-thick PET film as a substrate was cut to 2.5 × 2.5 cm^2, washed using acetone and 2-propanol, and dried with nitrogen gas. An IDE was deposited on the PET to fabricate a capacitor with 3 nm-thick Cr layer and 70 nm-thick Au layer, thermally deposited under ≈10^{-7} torr at the deposition rates of 0.2 and 7 Å s^{-1} using a shadow mask, respectively. The channel length and the width of IDE patterns were fixed to 200 and 26 000 µm, respectively, and the PhB/PVC sensing area was fixed to 5 × 5 mm^2. To improve spreading property of PhB/PVC solution on the substrate, the IDE-patterned PET substrate surface was exposed to 257 nm UV-ozone cleaner. Prior to this exposure, the part of the electrode connected to the external terminal was covered with polyimide (PI) tape. The prepared PhB/PVC solution filtered with a PVDF 0.45 µm filter was spin-coated on IDE at 1500 rpm for 180 s. A PhB/PVC film with a flat surface was fabricated at ≈15% humidity and a PhB/PVC film with a porous surface structure was fabricated at ≈60% humidity. Subsequently, the sample was dried in ambient condition for 2 h and then additionally dried in a vacuum condition for 1 h. After finishing the drying process, the finished capacitive LA sensors were kept in vacuum desiccator at room temperature.

Spectroscopic and Structural Analysis: UV–vis absorption spectra were recorded using a UV-vis spectrophotometer (Lambda 365, PerkinElmer). To analyze the solvatochromic behavior of PhB molecules, the PhB was dissolved in various solvents at a fixed concentration of 40 µM: CH, Tol, DCM, DMAC, DMF, DMSO, EtOH, 10 vol% EtOH solution in distilled water (DI water). The 10 vol% EtOH solution was used to increase the solubility of PhB, because PhB has low solubility in DI water. The absorbance variation of a solution (10 vol% EtOH) containing 100 mM LA and 40 µM PhB was analyzed after storing for various durations in the typical sealed cuvettes. Fourier-transform infrared spectroscopic analyses were performed using FT-IR 4600 spectrometer (JASCO) at 0, 24, 48, and 72 h by preparing the 100 mM LA solutions containing 40 µM PhB.

The 3D molecular orbital structure of the PhB molecule was simulated by DFT calculation (B3LYP/6-311G++(2dp)) using GAMESS (2020-R2), and the PhB molecular structure was also optimized using DFT calculation (B3LYP/6-311G++(2dp)). wxMacMolPlt graphics program was used. The PhB/PVC film morphology was visualized by atomic force microscopy (AFM, Digital Instruments MultiMode) via ex situ tapping-mode, field-emission scanning electron microscopy (Hitachi S-4200, FE-SEM). In AFM analysis, the SiN_x cantilever of the used Si tip has nominal constants and frequency values of 42 N m^{-1} and 320 kHz, respectively, and the tip radius was 10 nm. The PhB/PVC film thickness was measured using the alpha-step profilometer (Detak 150, Veeco) and PhB/PVC composite film thickness was measured to be 2.1 ± 0.3 µm. The surface energy (γ_s) of the PhB/PVC film was calculated using the below Owens-Wendt equation based on the contact angle (CA; θ) of the two probe liquids (DI water and diiodomethane) observed through a contact angle analyzer (Phoenix 300A, SEO Co., Inc.).

$$1+\cos\theta = \frac{2\left(\gamma_s^d\right)^{1/2}\left(\gamma_{lv}^d\right)^{1/2}}{\gamma_{lv}} + \frac{2\left(\gamma_s^p\right)^{1/2}\left(\gamma_{lv}^p\right)^{1/2}}{\gamma_{lv}} \quad (2)$$

Here, γ_s and γ_{lv} are the surface energies of the solid surface and the probe liquid, respectively, and the superscripts *d* and *p* indicate the dispersion and polar term of the surface energy, respectively.

Sensing Performance Characterization: The sensor capacitance was measured using an Agilent 4284 precision inductance–capacitance–resistance (LCR) meter at 10 kHz and 1 V. The sensor and LCR meter

© 2022 Wiley-VCH GmbH

16163028, 2023, 2, Downloaded from https://onlinelibrary.wiley.com/doi/10.1002/adfm.202211253 by Incheon National University, Wiley Online Library on [10/04/2023]. See the Terms and Conditions (https://onlinelibrary.wiley.com/terms-and-conditions) on Wiley Online Library for rules of use; OA articles are governed by the applicable Creative Commons License

were contacted using silver paste on the insulated wire. A polypropylene cylindrical chamber was used as the measurement chamber and the LA aqueous solutions with various concentrations were injected or removed with syringes. This schematic diagram is presented in Figure S4 (Supporting Information).

Supporting Information

Supporting Information is available from the Wiley Online Library or from the author.

Acknowledgements

This work was supported under the framework of international cooperation program (2021K1A3A1A20003483), the basic science research program (2022R1F1A1074088), and national R&D program (2022M3C1C3095083) managed by the National Research Foundation of Korea. The definition of the acronym DFT was changed from discrete fourier transform to density functional theory on January 10, 2023, after initial online publication.

Conflict of Interest

The authors declare no conflict of interest.

Data Availability Statement

The data that support the findings of this study are available from the corresponding author upon reasonable request.

Keywords

capacitive sensors, L-Lactic acid, phenol blue, sensing mediums, solvatochromism

Received: September 28, 2022
Published online: November 1, 2022

[1] Q. Liu, S. E. Bottle, P. Sonar, *Adv. Mater.* **2019**, *32*, 1903882.
[2] G. Choi, S. Oh, C. Kim, K. Lee, T. K. An, J. Lee, Y. Jang, H. S. Lee, *ACS Appl. Mater. Interfaces* **2020**, *12*, 32979.
[3] W. Shi, Y. Guo, Y. Liu, *Adv. Mater.* **2019**, *32*, 1901493.
[4] F. A. Viola, B. Brigante, P. Colpani, G. Dell'Erba, V. Mattoli, D. Natali, M. Caironi, *Adv. Mater.* **2020**, *32*, 2002329.
[5] R. Kubota, Y. Sasaki, T. Minamiki, T. Minami, *ACS Sens.* **2019**, *4*, 2571.
[6] Y. Fan, C. Zhang, Y. Du, C. Qiao, K. Wang, Y. Hou, J. Yao, Y. S. Zhao, *Adv. Funct. Mater.* **2021**, *31*, 2103031.
[7] S. Sudheendran Swayamprabha, D. K. Dubey, Shahnawaz, R. A. K. Yadav , M. R. Nagar, A. Sharma, F. Tung, J. Jou, *Adv. Sci.* **2020**, *8*, 2002254.
[8] J. Han, F. Bao, D. Huang, X. Wang, C. Yang, R. Yang, X. Jian, J. Wang, X. Bao, J. Chu, *Adv. Funct. Mater.* **2020**, *30*, 2003654.
[9] P. C. Y. Chow, T. Someya, *Adv. Mater.* **2019**, *32*, 1902045.
[10] W. Song, K. Yu, E. Zhou, L. Xie, L. Hong, J. Ge, J. Zhang, X. Zhang, R. Peng, Z. Ge, *Adv. Funct. Mater.* **2021**, *31*, 2102694.
[11] C. Yang, S. Zhang, J. Ren, M. Gao, P. Bi, L. Ye, J. Hou, *Energy Environ. Sci.* **2020**, *13*, 2864.
[12] C. Poriel, J. Rault-Berthelot, *Adv. Funct. Mater.* **2020**, *30*, 1910040.
[13] X. Yin, S. Sarkar, S. Shi, Q. Huang, H. Zhao, L. Yan, Y. Zhao, J. Zhang, *Adv. Funct. Mater.* **2020**, *30*, 1908445.
[14] G. Choi, S. Oh, J. Seo, H. S. Lee, *Adv. Funct. Mater.* **2020**, *30*, 2002979.
[15] E. Di Mauro, D. Rho, C. Santato, *Nat. Commun.* **2021**, *12*, 3167.
[16] S. Duan, T. Wang, B. Geng, X. Gao, C. Li, J. Zhang, Y. Xi, X. Zhang, X. Ren, W. Hu, *Adv. Mater.* **2020**, *32*, 1908388.
[17] Z. S. Miripour, F. Abbasvandi, P. Aghaee, S. NajafiKhoshnoo, M. Faramarzpour, P. Mohaghegh, P. Hoseinpour, N. Namdar, M. H. Amiri, H. Ghafari, S. Zareie, F. Shojaeian, H. Sanati, M. Mapar, N. Sadeghian, M. E. Akbari, M. A. Khayamian, M. Abdolahad, *Bioeng. Transl. Med.* **2021**, *7*, 10236.
[18] X. Hao, Y. Ren, M. Feng, Q. Wang, Y. Wang, *Biomed. Pharmacother.* **2021**, *141*, 111798.
[19] Y. M. Choi, H. Lim, H.-N. Lee, Y. M. Park, J.-S. Park, H.-J. Kim, *Biosensors* **2020**, *10*, 111.
[20] R. B. Rashid, X. Ji, J. Rivnay, *Biosens. Bioelectron.* **2021**, *190*, 113461.
[21] F. Alam, S. RoyChoudhury, A. H. Jalal, Y. Umasankar, S. Forouzanfar, N. Akter, S. Bhansali, N. Pala, *Biosens. Bioelectron.* **2018**, *117*, 818.
[22] R. Shiwaku, H. Matsui, K. Nagamine, M. Uematsu, T. Mano, Y. Maruyama, A. Nomura, K. Tsuchiya, K. Hayasaka, Y. Takeda, T. Fukuda, D. Kumaki, S. Tokito, *Sci. Rep.* **2018**, *8*, 6368.
[23] M. R. R. Khan, S. Oh, G. Choi, H. S. Lee, *Sens. Actuators, B* **2020**, *309*, 127783.
[24] W. Shi, Q. Li, Y. Zhang, K. Liu, X. Huang, X. Yang, Y. Ran, Y. Li, Y. Guo, Y. Liu, *Appl. Mater. Today* **2022**, *26*, 101275.
[25] K. Hiraka, K. Kojima, W. Tsugawa, R. Asano, K. Ikebukuro, K. Sode, *Biosens. Bioelectron.* **2020**, *151*, 111974.
[26] X. Liu, W. Zhang, Z. Lin, Z. Meng, C. Shi, Z. Xu, L. Yang, X. Y. Liu, *Small Methods* **2021**, *5*, 2000926.
[27] D. Jiang, C. Xu, Q. Zhang, Y. Ye, Y. Cai, K. Li, Y. Li, X. Huang, Y. Wang, *Biosens. Bioelectron.* **2022**, *210*, 114303.
[28] M. Adeel, M. M. Rahman, I. Caligiuri, V. Canzonieri, F. Rizzolio, S. Daniele, *Biosens. Bioelectron.* **2020**, *165*, 112331.
[29] J. Głowacka, R. Koncki, K. Strzelak, *Anal. Chim. Acta* **2022**, *1210*, 339878.
[30] S. Kim, K. Kim, H.-J. Kim, H.-N. Lee, T. J. Park, Y. M. Park, *Electrochim. Acta* **2018**, *276*, 240.
[31] S. G. Heo, W.-S. Yang, S. Kim, Y. M. Park, K.-T. Park, S. J. Oh, S.-J. Seo, *Appl. Surf. Sci.* **2021**, *555*, 149638.
[32] S. Wustoni, T. C. Hidalgo, A. Hama, D. Ohayon, A. Savva, N. Wei, N. Wehbe, S. Inal, *Adv. Mater. Technol.* **2019**, *5*, 1900943.
[33] Y. Zhang, D. Zheng, S. Liu, S. Qin, X. Sun, Z. Wang, C. Qin, Y. Li, J. Zhou, *Appl. Surf. Sci.* **2021**, *552*, 149529.
[34] C. Reichardt, *Solvents and Solvent Effects in Organic Chemistry*, Wiley-VCH, Weinheim **1988**.
[35] Z. Yoshida, F. Takabayashi, *Tetrahedron* **1968**, *24*, 933.
[36] W. Tao, M. Barra, *J. Chem. Soc., Perkin Trans. 2* **1998**, *2*, 1957.
[37] Y. Kimura, T. Yamaguchi, N. Hirota, *Phys. Chem. Chem. Phys.* **2000**, *2*, 1415.
[38] S. S. Khokhlova, V. A. Mikhailova, A. I. Ivanov, *Russ. J. Phys. Chem. B* **2007**, *1*, 443.
[39] T. Staline, N. Rajendiran, *Spectrochim. Acta, Part A* **2005**, *61*, 3087.
[40] T. Kobayashi, M. Shiga, A. Murakami, S. Nakamura, *J. Am. Chem. Soc.* **2007**, *129*, 6405.
[41] S. Oh, M. R. R. Khan, G. Choi, J. Seo, E. Park, T. K. An, Y. D. Park, H. S. Lee, *ACS Appl. Mater. Interfaces* **2021**, *13*, 56385.
[42] N. A. Mohamed Safian, A. Anuar, A.-Z. Omar, T. M. Bawazeer, N. Alsenany, M. S. Alsoufi, A. Supangat, N. A. Roslan, *Sens. Actuators, B* **2021**, *343*, 130158.
[43] G. J. M. Koper, M. H. P. van Genderen, C. Elissen-Román, M. W. P. L. Baars, E. W. Meijer, M. Borkovec, *J. Am. Chem. Soc.* **1997**, *119*, 6512.
[44] K. Hirano, H. Yamato, K. Kunimoto, M. Ohwa, *Bull. Chem. Soc. Jpn.* **2001**, *74*, 2369.

© 2022 Wiley-VCH GmbH

16163028, 2023, 2, Downloaded from https://onlinelibrary.wiley.com/doi/10.1002/adfm.202211253 by Incheon National University, Wiley Online Library on [10/04/2023]. See the Terms and Conditions (https://onlinelibrary.wiley.com/terms-and-conditions) on Wiley Online Library for rules of use; OA articles are governed by the applicable Creative Commons License

[45] D. Peeters, G. Leroy, C. Wilante, *J. Mol. Struct.* **1997**, *416*, 21.
[46] L. Long, M. Huang, N. Wang, Y. Wu, K. Wang, A. Gong, Z. Zhang, J. L. Sessler, *J. Am. Chem. Soc.* **2018**, *140*, 1870.
[47] J. -F. Li, Z. -L. Xu, H. Yang, *Polym. Adv. Technol.* **2008**, *19*, 251.
[48] H. -L. Qian, W. -P. Huang, Y. Fang, L. -Y. Zou, W. -J. Yu, J. Wang, K. -F. Ren, Z. -K. Xu, J. Ji, *ACS Appl. Mater. Interfaces* **2021**, *13*, 57000.
[49] J. Vial, A. Jardy, *Anal. Chem.* **1999**, *71*, 2672.

© 2022 Wiley-VCH GmbH

16163028, 2023, 2, Downloaded from https://onlinelibrary.wiley.com/doi/10.1002/adfm.202211253 by Incheon National University, Wiley Online Library on [10/04/2023]. See the Terms and Conditions (https://onlinelibrary.wiley.com/terms-and-conditions) on Wiley Online Library for rules of use; OA articles are governed by the applicable Creative Commons License